Available online at www.sciencedirect.com
ScienceDirect
Journal of Photochemistry and Photobiology A: Chemistry 190 (2007) 290–300
Journal of Photochemistry and Photobiology A:Chemistry
www.elsevier.com/locate/jphotochem

Exciting flavins: Absorption spectra and spin–orbit coupling in light–oxygen–voltage (LOV) domains

Karl Zenichowski, Marcel Gothe, Peter Saalfrank *

Theoretische Chemie, Institut für Chemie, Universität Potsdam, Karl-Liebknecht-Straße 24-25, D-14476 Potsdam-Golm, Germany

Received 24 November 2006; received in revised form 5 February 2007; accepted 11 February 2007
Available online 17 February 2007

Abstract

Flavins are central molecular chromophores for many photobiological processes. In this paper, several aspects of the photophysics and photochemistry of lumiflavin in a (protein) environment will be studied with the help of quantum chemical methods. In a first part of the paper, we present vertical singlet excitation energies for lumiflavin (a molecule of the isoalloxazin type), using time-dependent density functional theory (TD-DFT) in conjunction with the B3LYP hybrid functional. When calculated for isolated species, TD-DFT excitation energies are generally blue-shifted relative to the experimental absorption spectra of isoalloxazines in solution, or in a protein environment. We develop four different models to account for environmental effects, with special emphasis on the LOV1 domain of *Chlamydomonas reinhardtii*. It is found that the two lowest, allowed singlet excitations are sensitive to the polarizability of an environment, to hydrogen bonds, and to geometrical constraints imposed by the surrounding protein. All of this brings theory and experiment in better agreement.

In the second part of the paper the light-induced adduct formation in LOV domains, between the chromophore and a neighbouring cystein unit is investigated. Energies along a model "reaction path" are calculated on the DFT/B3LYP and MCQDPT2 level of theories. A transition state for a H-transfer between the mercapto (SH–) group of cystein, and the N(5) position of flavin is found. The reaction requires spin–orbit coupling between the S_0 and the T_1 states of the system. Spin–orbit coupling constants between S_0 and T_1 are calculated, and found to be in the range of several tens of cm^{-1} after the transition state was passed. A biradical intermediate was observed along the reaction path.

Keywords: Isoalloxazin; Time-dependent DFT; LOV domains; Photo-cycle; Spin–orbit coupling

1. Introduction

Sunlight is the primary source of energy on earth, as well as a fast carrier of information. As a consequence, a fascinating variety of protein embedded photoreceptor molecules is provided by nature. For higher plants, three classes of photo-switchable receptors are known, termed phytochromes, cryptochromes, and phototropins [1]. Phototropin receptors, are, for example, involved in phototropic response, guard cell regulation, and chloroplast relocation [2]. Phototropins consist of three domains, two LOV (light-, oxygen-, voltage-sensitive) domains and a C-terminal kinase domain. Each LOV domain contains a non-covalently bound flavin mononucleotide (FMN) as the photoactive chromophore. During recent years, phototropins were found in many organisms [3]. It is a common feature of LOV domains to undergo a photocycle after blue-light excitation. The LOV1 domain from the single cellular green algae *Chlamydomonas reinhardtii*, for example, shows the following reaction cycle [4]. The dark, or educt state (LOV1-447, singlet[1]) is transferred, after blue-light excitation, *via* an intermediate triplet (LOV1-715), towards the transient signaling, or adduct state (LOV1-390, singlet). This state consits of the FMN molecule covalently bound, to a neighbouring cystein residue, *via* its C(4a) position [5]. A dark reaction completes the cycle, which is illustrated schematically in Fig. 1 and which will be discussed in some greater detail below.

* Corresponding author. Tel.: +49 331 9775232; fax: +49 331 9775058.
E-mail addresses: peter.saalfrank@rz.uni-potsdam.de, petsaal@rz.uni-potsdam.de (P. Saalfrank).

[1] The notion 447 refers to the lowest-energy absorption band, at $\lambda = 447$ nm.

1010-6030/$ – see front matter © 2007 Elsevier B.V. All rights reserved.
doi:10.1016/j.jphotochem.2007.02.007

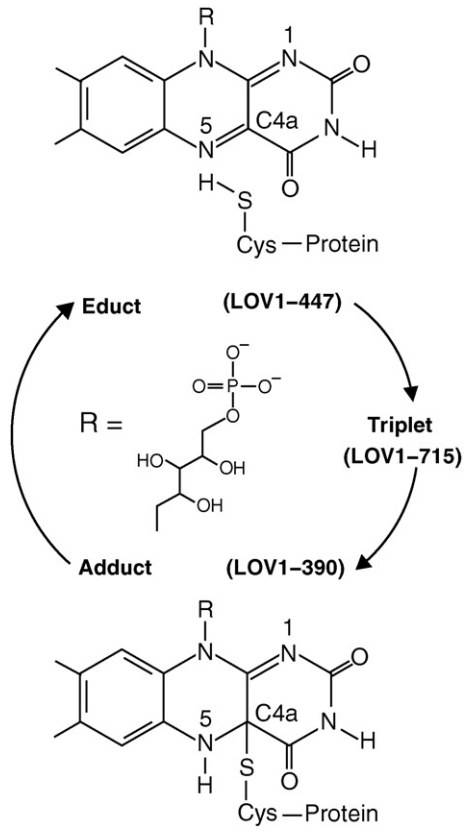

Fig. 1. Photocycle in the LOV1 domain of *Chlamydomonas reinhardtii* (schematically after [4]).

1.1. Absorption spectra of LOV domains

The absorption properties of LOV1-447 are nearly identical for the LOV domains from *Avena sativa* [6] and *Adiantum capillus veneris* [7]. Accordingly, absorption bands centered around 450 nm and 360 nm, are found corresponding to $S_0 \rightarrow S_1$ and $S_0 \rightarrow S_2$ transitions (and an intense band $S_0 \rightarrow S_3$ around 270 nm) [4,8]. Apart from earlier semiempirical calculations on the absorption spectra of isoalloxazine-type molecules [9–11],

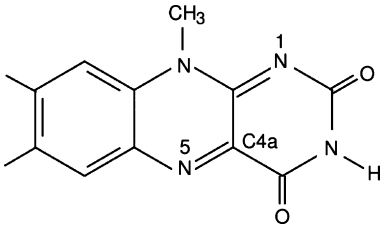

Fig. 2. Lumiflavin in its oxidized form (7,8,10-trimethyl-isoalloxazin).

several newer, first-principles calculations exist, most of them based on TD-DFT [12] in conjunction with the B3LYP hybrid exchange-correlation functional [13]—see Refs. [14–16]. In these papers, the spectra were calculated for isolated molecules, and environmental effects were largely neglected.

This earlier obtained TD-DFT results demonstrate the overall $\pi \rightarrow \pi^*$-character for the visible excitations, and show already a fairly good agreement with experimental data. However, the TD-DFT excitation energies are blue-shifted relative to experiment by several tenths of an electron volt (eV). For 7,8,10-trimethyl-isoalloxazin (lumiflavin, oxidized form), for example, which is shown in Fig. 2, the three strongest peaks are, with TD-DFT(B3LYP)/6-31G(d), at 3.04 eV (408 nm, S_1), 3.86 eV (322 nm, S_2), and 4.91 eV (253 nm, S_3) [14]. The corresponding experimental values, for lumiflavin in water, are 2.79 eV (445 nm), 3.38 eV (367 nm) [17], and 4.59 eV (270 nm) [18]—see also Table 1. The spectrum of lumiflavin in water is very similar to those of the above-mentioned LOV1-447 domains, except that a vibrational fine structure exists for the S_1 band in the protein environment [4].

Possible reasons for the mismatch between theory and experiment, are geometrical distortions or other effects due to the environment, and methodological aspects such as static correlation, basis set effects, and the reliability of the B3LYP functional. Concerning the latter, it was found that TD-DFT in conjunction with hybrid exchange-correlation functionals such as BLYP or B3LYP typically underestimate (by about 0.2 eV), rather than overestimate, excitation energies [19,20]. The B3LYP func-

Table 1
TD-DFT(B3LYP)/6-31G(d) vertical singlet excitation energies for flavin-protein models A–D in eV, along with oscillator strengths

	A		B		C		D		Experimental	
	E_i (eV)	f_i	E_i (eV)	f_i	E_i (eV)	f_i	E_i (eV)	f_i	(a)	(b)
$S_0 \rightarrow S_1$										
($\pi \rightarrow \pi^*$)	**3.04**	**0.190**	**2.98**	**0.235**	**2.88**	**0.237**	**2.90**	**0.186**	**2.77**	**2.79**
($n \rightarrow \pi^*$)	3.09	0.000	3.28	0.000	3.02	0.002	3.25	0.001		
($n \rightarrow \pi^*$)	3.30	0.000	3.40	0.000	3.24	0.001	3.30	0.001		
($n \rightarrow \pi^*$)	3.84	0.000					2.41	0.000		
$S_0 \rightarrow S_2$										
($\pi \rightarrow \pi^*$)	**3.86**	**0.134**	**3.72**	**0.213**	**3.70**	**0.162**	**3.55**	**0.168**	**3.44**	**3.38**
⋮	⋮	⋮	⋮	⋮	⋮	⋮	⋮	⋮		
$S_0 \rightarrow S_3$										
($\pi \rightarrow \pi^*$)	**4.91**	**0.592**	**4.86**	**0.743**	**4.60**	**0.489**	**4.59**	**0.492**	**4.63**	**4.59**

The dominant transitions (S_1, S_2, S_3) are shown in bold. Experimental data, taken from literature, are shown in the last two columns: (a) FMN in the LOV1 domain of *Chlamydomonas reinhardtii* [4]. (b) Lumiflavin (in H_2O) [17,18]. If no entries are shown, the states do not exist or are shifted in the particular model. The vertical dots indicate that a number of further singlet states exist between S_2 and S_3, which are not listed.

tional cannot therefore explain the observed blue-shift relative to the experiment. The basis set error, for isoalloxazin-type molecules, was also found to be small [16]. For uracil, on the other hand, which shares with alloxazines its pyrimidin moiety, a systematic study has shown that extended bases lead to a red-shift of the most intense transitions: for the two lowest high-intensity transitions one finds a shift by 0.2 eV and 0.14 eV, respectively, when going from TD-DFT(B3LYP)/6-31G(d) to TD-DFT(B3LYP)/aug-cc-pVTZ [14]. The possible multi-reference character of excited states has also been tested for lumiflavin [14], by using a combined density functional theory/multireference configuration method (DFT/MRCI) [21]. In this study, only small differences ≤ 0.08 eV were found between DFT/MRCI and TD-DFT. Altogether, a blue-shift remains and effects other than those related to the method should be examined. This is corroborated by the observed, better agreement of experimental and theoretical spectra for uracil in the gas phase [14].

Therefore, in the following, we focus on solvation and embedding effects as a possible explanation for the observed blue-shift in theory. Experimentally, solvent effects for the lumiflavin singlet absorption spectra have been systematically studied [17]. The spectra show a clear dependence on the solvent polarity, and the capability of the environment to form hydrogen-bonds with the chromophore, which both affect the position in particular of the S_2 band. We were able to reproduce this experimentally observed trends, as we will show later on. The influence of a solvent was also theoretically addressed, on the basis of semiempirical calculations [22]. More recently, TD-DFT calculations on isolumazin with three water molecules attached to the pyrimidin site of isolumazin, showed a decrease in excitation energy for the $S_0 \rightarrow S_2$ transition by about 0.1 eV [14].

What is still missing, is a systematic study of solvent effects on the first-principles level, a more quantitative analysis relevant also to flavins in biological systems, and a detailed understanding which environmental effect leads to which effect on which band. To this end, we choose the LOV1 domain of *C. reinhardtii* as an example to study effects of the protein binding pocket in which flavin is embedded. Detailed crystal structure data provide the framework for possible hydrogen bonding interactions and geometrical constraints imposed on the flavin molecule by the protein [5].

1.2. Adduct formation and spin–orbit coupling

A second goal of this paper is to address details of the photocycle in LOV domains after blue-light absorption in lumiflavin, as sketched in Fig. 1. Accordingly, after photoexcitation two intersystem crossings (ISC) occur during adduct formation [4]. First, FMN (LOV1-447, S_0) is photoexcited to (a) photoexcited singlet state(s), and then converted by ISC to the intermediate triplet state (LOV1-715, T_1), on a nanosecond timescale. During the second ISC event, the triplet decays back to the singlet ground state. In the LOV domain wildtype this second ISC is accompanied by formation of the adduct (LOV1-390, S_0), and takes place on a microsecond timescale. The triplet lifetime becomes longer in cases of hindered adduct formation, caused by substitution of the cystein residue close to FMN in mutation experiments, e.g., by serin [23]. In cases where the photocycle is not interrupted at the stage of the photoadduct, it is completed by the dark reaction which proceeds on the timescale of minutes, and which recreates the LOV1-447 form—the photocycle can start again.

Since ISC is central for the photocycle in LOV domains, the question about the detailed mechanism of spin–orbit coupling and adduct formation arises. The present work supports a scenario in which a radical pair is formed in the triplet state, followed by ISC to the singlet ground state and radical recombination. The experimental characterization of oxidizing isoalloxazin triplet species, generated *via* photoexcitation, is known for a long time [24]. Transient triplet radical pairs were observed for example by EPR, ENDOR and NMR studies on single-point mutated, non-adduct forming LOV domains [6,25–27]. Theoretical model studies for adduct formation in the gas phase [28], and a QM/MM approach have been presented [29]. Both studies propose an initial hydrogen transfer, from the cystein-SH position to the N(5)-FMN site (see Fig. 1). The resulting neutral biradical, of triplet character, was stated to be favourable for adduct formation. Recently published results for CASSCF/MCQDPT2 based calculations, concerning the energy profile of adduct formation, further underlined this mechanism [30]. Our study, however, is focused on spin–orbit coupling and discusses the underlying mechanisms on an orbital level.

Strong spin–orbit coupling between S_0 and T_1 potential energy surfaces, for the biradical state, was conjectured by experiment and theory [6,29]. To confirm the proposed suggestion, calculations of spin–orbit coupling, within a multi-reference approach, are presented in the present work.

The paper is organized as follows. After this section, the next section describes methods and computational details by which the absorption spectra for the educt state (Section 2.1), and spin–orbit couplings along a simplified reaction path (Section 2.2), have been calculated. In Section 3 we present and discuss results, first for the absorption spectra (Section 3.1), then for spin–orbit coupling during adduct formation (Section 3.2). A final Section 4 concludes this work.

2. Methods and computational details

2.1. TD-DFT absorption spectra

We calculated vertical singlet TD-DFT excitation energies and oscillator strengths, out of the fully or partially DFT-optimized singlet ground state (S_0) of lumiflavin, plus surrounding molecular units, if considered. Geometry optimizations and calculation of excitation energies were done with the B3LYP functional [13], and a valence split polarized 6-31G(d) basis set [31]. The 6-31G(d) basis in combination with B3LYP is known to give reasonable results for both, excitation energies of isoalloxazin type molecules [14,16,17], and geometries optimized in their ground state [32,33].

We performed polarizable continuum model (PCM) calculations, using the integral equation formalism mode (IEF-PCM) to simulate the polarizability of a solvent [34]. The radii for the enclosing spheres containing the point charges, were taken

from the United Atom for Hartree Fock (UAHF) dataset [35]. The enclosing surface was created by the GEnerating POLyhedra (GEPOL) algorithm [36]. Chloroform was taken as a solvent for most PCM calculations below; the corresponding dielectric constant of $\epsilon = 4.9$ is reasonable also for proteins [37]. For the calculations, the Gaussian03 program package was used [38].

The line spectra obtained by TD-DFT were artificially broadened by Gaussians, centered around wavelength λ_i, with oscillator strength f_i,

$$I(\lambda) = C\sum_i f_i \, \mathrm{e}^{-(1/2)((1/\lambda)-(1/\lambda_i)/\sigma)^2} \quad (1)$$

where $C = (\sigma\sqrt{2\pi})^{-1}$ normalizes each Gaussian to 1, to account for line broadening caused by finite lifetime, rotational motion, inhomogeneities, etc. The Gaussian width σ was set to $1000\,\mathrm{cm}^{-1}$ for all spectra below. Extinction coefficients were calculated as $\varepsilon(\lambda) = \kappa I(\lambda)$, where $\kappa = 4m_\mathrm{e}c^2\epsilon_0 \ln(10)/(Le^2) = 4.318998 \times 10^{-10}$ mol/m (m_e is the electron mass, c the velocity of light, ϵ_0 the vacuum dielectric constant, L the Avogadro's constant and e is the electron charge).

2.2. MCQDPT2 calculations for adduct formation

The MCQDPT2 (2nd order multiconfiguration quasi-degenerate perturbation theory) [39,40] as implemented in the GAMESS quantum chemistry package [41], was used in the following to estimate the spin–orbit coupling along an approximate reaction path for adduct formation after illumination of FMN. MCQDPT2 is a multistate and multireference approach, including second order perturbative corrections. It efficiently describes static and dynamic correlation for ground and excited states. With the help of the SO-MCQDPT2 [42] program, which also comes with GAMESS, spin–orbit coupling is included within a multireference perturbative approach. The different spin-states are allowed to mix *via* an effective Hamiltonian which consists of spin dependent and spin independent parts. Both parts include non-perturbed as well as perturbed (second-order) contributions. Since traditional perturbation theory is applicable only for single states, the perturbative treatment of the spin-dependent Hamiltonian [43] is carried out within the framework of quasi-degenerate perturbation theory [44]. The spin–orbit coupling is treated on the basis of the Breit-Pauli coupling Hamiltonian. The applied spin–orbit coupling operator fully captures one-electron terms, *i.e.*

$$\hat{H}_\mathrm{so}^{(1)} = \frac{e^2}{2m_\mathrm{e}^2c^2}\sum_i^N\sum_{A=1}^{N_A}\frac{Z_A}{|\underline{r}_i - \underline{R}_A|^3}\hat{\underline{l}}_{iA}\hat{\underline{s}}_i \quad (2)$$

where N is the number of electrons, N_A the number of nuclei (with nuclear charge Z_A), $|\underline{r}_i - \underline{R}_A|$ the distance between electron i and nucleus A and $\hat{\underline{l}}_{iA} = (\underline{r}_i - \underline{R}_A) \times \underline{\hat{p}}_i$, $\hat{\underline{s}}_i$ is the spin operator of electron i. Two-electron contributions $\hat{H}_\mathrm{so}^{(2)}$ to the total spin–orbit coupling operator $\hat{H}_\mathrm{so}$, spin–same orbit and spin–other orbit contributions, were included in an approximate way, by only treating so called core-active terms [42,45]. The formalism was applied here to calculate the S_0–T_1 and S_1–T_1 spin–orbit coupling terms, $\langle\Psi_{T_1}|\hat{H}_\mathrm{so}|\Psi_{S_n}\rangle =: \langle T_1|\hat{H}_\mathrm{so}|S_n\rangle$.

For this purpose, single-point MCQDPT2/6-31G(d) calculations were carried out on an initial RHF/6-31G(d) orbital set. The RHF calculations were done for five geometries A–E optimized at the (U)B3LYP/6-31G(d) level of theory, and resembling various points along an approximate reaction path which connects the educt with the adduct state (see below). The RHF orbital set was used to obtain the lowest two CAS-CI states, independently for singlet and triplet multiplicity. An active space of three occupied and three virtual orbitals was chosen. Single point energies were obtained after additional second order perturbative treatment of the CAS-CI states. The energetically lowest states obtained in this way are S_0 and T_1, respectively, with wavefunctions Ψ_{S_0} and Ψ_{T_1}.

To obtain a transition state along the reaction path on the T_1 surface, the Synchronous Transit-Guided Quasi-Newton (STQN) method [46] implementation in the Gaussian03 package, called QST3, was used. Further steps along the reaction path were generated *via* the intrinsic reaction coordinate (IRC) method [47], also with Gaussian03, but are not shown here (see below).

3. Results and discussion

3.1. Absorption spectra

3.1.1. Absorption spectra for various environments

To analyse effects of solvation and protein environment on the spectra of flavin-type molecules, four different models A–D were examined on the (TD-)DFT(B3LYP)/6-31G(d) level of theory. The different models are[2]

A. The gas phase lumiflavin molecule (in its oxidized form), as shown in Fig. 2, in its singlet ground state S_0. The lumiflavin geometry was B3LYP/6-31G(d) optimized in the gas phase.
B. Model B is model A, plus a PCM field which was applied during the TD-DFT calculation. If not stated otherwise, chloroform was used as a solvent ($\epsilon = 4.9$), which also serves to simulate the dielectric constant of proteins in the range of 2–4 [37]. Other solvents (cyclohexane, $\epsilon = 2.0$; ethanol, $\epsilon = 24.6$; water, $\epsilon = 78.4$) were also considered. Geometries were always those of model A—reoptimization in the PCM field led to only tiny differences of less than 0.01 Å in bond lengths and less than 1° for bond angles.
C. Model C is model B (with chloroform as solvent), however, with the lumiflavin geometry taken from the LOV1 domain crystal structure of *C. reinhardtii* in its dark state [5]. The geometrical changes from B to C are discussed below.
D. Model D consists of lumiflavin in the crystal adapted geometry of C and additional seven aminoacid sidechains, which were reduced for simplicity to their functional groups (see Fig. 3). The H-atoms in models C and D were placed manually and B3LYP/6-31G* optimized in their cartesian

[2] Coordinates availible on request: zenichow@rz.uni-potsdam.de.

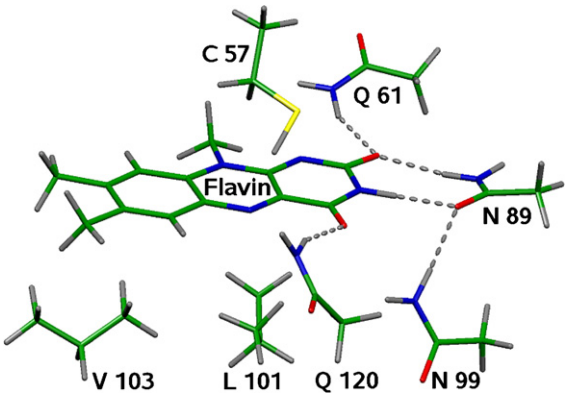

Fig. 3. Model D: lumiflavin with surrounding aminoacid side chains Cys 57, Val 103, Leu 101, Asn 89, Asn 99, Gln 120 and Gln 61, all based on the crystal structure of *C. reinhardtii* [5], only H atom coordinates were optimized with B3LYP/6-31G(d). Hydrogen bonds are shown as dotted lines.

coordinates afterwards. For the TD-DFT calculation, the whole structure was enclosed in the PCM field of chloroform. According to the LOV1 crystal structure, four of the aminoacids, Gln 61, Asn 89, Gln 120, and Asn 99 form hydrogen bonds to the pyrimidin site of FMN. Finally, the Cys 57 residue which is involved in adduct formation, was included. The coordinates for the flavin molecule and the aminoacid side chains were taken again from the crystal structure of the LOV1 domain [5]. The resulting structure of model D is shown in Fig. 3. In passing we note that in a further model, D', the methyl group in N(10) position was replaced by a CH_2CH_2OH group, as a more realistic substitute of the ribityl chain. Since this modification led only to minor differences in the computed spectra of model D, model D' is not further considered here.

In Fig. 4 we show the (broadened) TD-DFT(B3LYP) spectra out of the S_0 state of lumiflavin (along with the line spectrum), for models A–D. Further, in Table 1 singlet excited states are provided for all models, with oscillator strengths and excitation energies also for dark states indicated.

For model A our TD-DFT calculations reproduce the overall $\pi \rightarrow \pi^*$ character for the visible excitations, the excitation energies and oscillator strengths, obtained for lumiflavin and TD-DFT by Sikorska et al. [17] and Neiss et al. [14]. From Fig. 4 and Table 1 we note that, while model A shows the observed blue-shift for all visible bands, the most sophisticated model D is in almost quantitative agreement with the experimental observations for LOV1-447 of *C. reinhardtii*. In particular for model D, S_1 is shifted, relative to model A, by 0.14 eV or 1130 cm^{-1} (from 408 nm (3.04 eV) to 428 nm (2.90 eV)), S_2 is shifted by 0.31 eV or 2500 cm^{-1} (from 321 nm (3.86 eV) to 349 nm (3.55 eV)), and S_3 by 0.32 eV or 2580 cm^{-1} (from 252 nm (4.91 eV) to 270 nm (4.59 eV)). The remaining error, for model D, in theory is at most 0.13 eV. The error accounts for intrinsic errors of method, functional and basis set. Furthermore, model D still represents a simplified model with lumiflavin instead of FMN and 7 aminoacid fragments instead the real protein binding pocket.

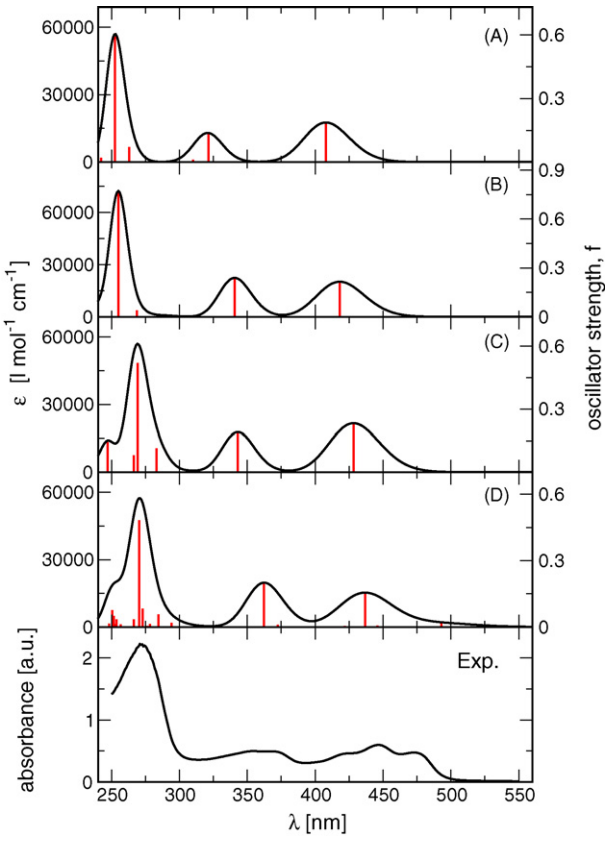

Fig. 4. Calculated oscillator strengths f_i (right scale, sticks), extinction coefficients $\varepsilon(\lambda)$ (left scale, solid line) as a function of excitation wavelength λ (in nm) for the four different flavin-protein models A–D (TD-DFT(B3LYP)/6-31G(d)). The experimental absorption spectra for the LOV1 domain of *C. reinhardtii* in its dark state, as shown in the bottom, was adapted from Ref. [4].

In passing we note that as a further difference between models A–C on the one side, and D on the other, we find a number of low-energy excitations for the latter, in the range from 2.1 to 2.8 eV, below S_1. These show small oscillator strengths, and are due to charge transfer excitations from occupied orbitals of the aminoacids into low-lying π^* orbitals of lumiflavin. Since excitation energies for charge transfer states may well be underestimated by the present TD-DFT method [48], and since these states play no role for the photophysics, they are not listed in Table 1 and will not be further discussed.

One also finds $n \rightarrow \pi^*$ transitions, with low oscillator strengths, energetically located between S_1 and S_2. Previous TD-DFT calculations for gas phase lumiflavin (similar to our model A), showed the lowest $\pi \rightarrow \pi^*$ (S_1) and $n \rightarrow \pi^*$ transitions are energetically very close [16]. This was interpreted of being indicative for the so-called *proximity effect* [49]. Accordingly, the energetically close states are strongly vibronically coupled, thus affecting the photophysical properties of isoalloxazines in dependence of solvent, substituent and temperature [16,50,51]. For model A (gas phase), we find the smallest energy gap between $\pi \rightarrow \pi^*$ and $n \rightarrow \pi^*$ of 0.05 eV, which increases to about 0.3 eV in model B. This was interpreted as a progressive weakening of the proximity effect in solvents with increasing polarity, resulting in a lower non-radiative decay rate of excited

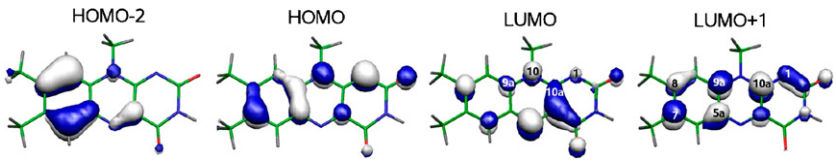

Fig. 5. TD-DFT(B3LYP)/6-31G(d) orbitals for lumiflavin in the S_0 state (model B).

singlets for the latter [51]. For models C and D, which resemble the situation for LOV1-447 of *C. reinhardtii* more closely, the gap is 0.14 eV and 0.19 eV, respectively, *i.e.* non-radiative decay of state S_1 should be more efficient again in the protein environment, compared to solution.

Returning to the model-dependence of the visible S_1, S_2 and S_3 bands, the following observations are made. When going from models A to B, S_1 and S_2 are red-shifted by about 0.06 eV and 0.14 eV, respectively. The S_1 band is dominated by the HOMO → LUMO transition in models A and B, and only weakly affected by the polarizable solvent: the HOMO–LUMO gap decreases from A to B by approximately 0.02 eV. The (small) red-shift is also caused by the strong destabilization of the HOMO-2 π orbital (by 0.13 eV), which contributes to the S_1 excitation. The destabilization of this π orbital is due to its larger coefficients at the unpolar dimethyl-benzene moiety of isoalloxazin in comparison to the HOMO (LUMO) orbitals. HOMO-2, HOMO and LUMO for model B are plotted in Fig. 5. The S_2 band, on the other hand, is dominated by transitions out of the, former mentioned, HOMO-2 orbital into LUMO. This explains the larger red-shift of about 0.14 eV for S_2. The intense absorption band S_3 is red-shifted by about 0.05 eV from A to B.

That the solvent polarity affects mostly S_2, not so much S_1 and S_3, is also demonstrated in Table 2, giving excitation energies and oscillator strengths for various PCM fields. It is seen that S_2 is red-shifted the more, the more polar the solvent is. This is in agreement with experimental observation [17], and is interpreted here as being due to the destabilization of occupied π orbitals by the solvent. Note that the agreement (for water) between theory and experiment is still not good for S_2 and S_3, simply because in model B no hydrogen-bonds nor geometrical constraints have been accounted for.

When going from models B to C we take, on top of the polarizability of the environment, also the geometrical distortion of the chromophore in the protein environment of *C. reinhardtii* into account. By comparing bond lengths, it is found that these are generally slightly extended in the crystal compared to the free molecule. The largest deviations of 0.05–0.07 Å involve the N(1)–C(10a), N(10)–C(9a), C(5a)–C(9a), C(5a)–C(6) and the C(7)–C(8) bonds (Fig. 5). While the accuracy of the crystal structure is limited [52], the B3LYP geometries are typically more accurate than the differences observed here [53]. We conclude that the stated differences between the gas phase optimized lumiflavin and the crystal structure are caused by interactions between flavin moiety and the surrounding protein.

Due to bond elongation, the S_1 absorption, in model C, red-shifts by 0.1 eV compared to model B. A simple picture is that a $\pi \rightarrow \pi^*$ transition, when idealized in a particle-in-the-box model, is lowered in energy when the box is enlarged. A more sophisticated picture arises from inspection of the LUMO in Fig. 5. It is found that antibonding interactions, for example between atoms C(9a) and N(10), N(10) and C(10a), and C(10a) and N(1), are reduced when the corresponding bonds stretch. As a consequence, the LUMO is stabilized and the HOMO–LUMO gap, which dominates the transition also in model C, is reduced.

Similarly, in model C the intense absorption band S_3, around 250 nm, is shifted to lower energies by about 0.26 eV, compared to B. Since this transition is dominated by a HOMO → LUMO + 1 excitation, this effect can be traced back to the observed stabilization (by 0.3 eV) of LUMO + 1 (see Fig. 5). Again, antibonding interactions are reduced by bond elongation. Finally, the S_2 peak is also red-shifted, but only by a tiny amount, because contributing occupied and unoccupied orbitals are nearly equally stabilized from B to C.

This is different when going from models C to D, where we find a significant red-shift of about 0.15 eV for the S_2 band. In this model, four amino acids Asn 89, Asn 99, Gln 120, and Gln 61 form hydrogen bonds with the pyrimidin unit of flavin, see Fig. 3. This stabilizes the LUMO through non-vanishing coefficients at the oxygen atoms of the pyrimidin unit (see Fig. 7). In model D,

Table 2
Excitation energies and oscillator strengths for the visible transitions of lumiflavin, in dependence of the PCM solvent (model B), in comparison to the gas phase values (model A), and experiment (lumiflavin, H_2O) [17,18]

	Model A (gas phase)	$\epsilon = 2.02$ (cyclohex.)	$\epsilon = 4.9$ (chloroph.)	$\epsilon = 24.55$ (ethanol)	$\epsilon = 78.39$ (water)	Experiment
$S_0 \rightarrow S_1$						
E_i (eV)	3.04	2.99	2.98	2.97	2.97	2.79
f_i	0.190	0.241	0.235	0.231	0.219	
$S_0 \rightarrow S_2$						
E_i (eV)	3.86	3.77	3.72	3.68	3.64	3.38
f_i	0.134	0.196	0.213	0.229	0.242	
$S_0 \rightarrow S_3$						
E_i (eV)	4.91	4.85	4.86	4.85	4.86	4.59
f_i	0.592	0.713	0.743	0.763	0.775	

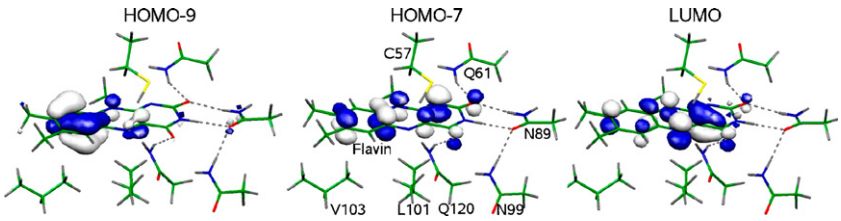

Fig. 6. TD-DFT(B3LYP)/6-31G(d) orbitals for lumiflavin and surrounding side chains (model D) in the S_0 state, see caption of Fig. 3 for a detailed description.

the $S_0 \rightarrow S_2$ transition is dominated by a HOMO-9 → LUMO excitation. The energy gap between LUMO and HOMO-9 is reduced by 0.15 eV since H-bonding affects HOMO-9 to a lesser extent than the LUMO, leading to the observed red-shift. In contrast, the positions of S_1 and S_3 absorption bands are only slightly affected by H-bonds. The fact that S_1 is so unsensitive may be surprising in view of the stabilized LUMO, and the further reduction of the HOMO-LUMO gap (by 0.14 eV) when going from C to D. Closer inspection shows, however, that in model D the S_1 band is dominated by a HOMO-7 → LUMO transition. The gap between LUMO and HOMO-7 changes only slightly, hence there is no shift of the S_1 band. The orbitals are shown in Fig. 6.

In summary we find that red-shifts for all visible peaks occur due to the environment. In particular, (i) polar solvents shift S_2, to a somewhat lesser extent also S_1, (ii) bond elongation in the crystal environment affects S_3, to a lesser extent also S_1 and (iii) hydrogen bonding affects almost exclusively the S_2 band. The effects can be rationalized based on the shape of the molecular orbitals involved in the transitions, which are influenced differently by different environmental effects.

3.1.2. Further investigations

Two further aspects of the absorption spectra of LOV domains were addressed, namely the vibrational fine structure in the S_1 band of LOV1 of *C. reinhardtii* [4], and the absorption spectrum of a mutant, C57M, in which the H atom in Cys 57 had been replaced by a methyl group [54].

3.1.2.1. Vibrational fine structure of the S_1 band of LOV1-447. The S_1 (447 nm, 2.77 eV) band of LOV1 of *C. reinhardtii* is superimposed by three peaks, with an energy spacing of about 1250 cm^{-1} [4]. We performed, for the free lumiflavin molecule, frequency analyses in the geometry-optimized S_0 and S_1 states, on the RHF/6-31G(d) (S_0) and CIS/6-31G(d) (S_1) level of theories. The RHF frequencies were scaled by a factor of 0.8929 [55], the CI frequencies by 0.9 [56,57]. Since $S_0 \rightarrow S_1$ is dominated by the HOMO → LUMO transition, an inspection of the frontier orbitals is useful.

It is found that the HOMO is C(5a)–C(9a) bonding and C(4a)–C(10a) non-bonding, while the LUMO is C(5a)–C(9a) non-bonding and C(4a)–C(10a) bonding (see Fig. 5 for the B3LYP case). In fact one finds in the frequency analyses a stretching mode involving the C(5a)–C(9a) and C(4a)–C(10a) atom pairs, which is located (scaled values) at 1278 cm^{-1} (S_0) and 1295 cm^{-1} (S_1), respectively. It can therefore be concluded, that the vibrational fine structure arises from C–C vibrations located at the central six-ring of FMN.

3.1.2.2. Absorption spectra of a mutant, C57M. When the H atom in Cys 57 is replaced by a methyl group (C57M mutant), the photoexcitation of the LOV1-C57M dark form in *C. reinhardtii* has been found to lead to different reaction products in comparison to the wildtype [54]. Accordingly, blue-light absorption first creates, through excited singlets and an intermediate triplet, an adduct C57M-415. This species has been interpreted as a reaction product in which the $–CH_2–S–CH_2–$protein unit has been added to N(5) (not C(4a)), and H–C(4a) (not N(5)). Further, after thermal conversion a C57M-675 species was formed out of C57M-415, which was speculated as being a radical, generated from C57M-415 by abstraction of the H atom from C(4a).

This latter hypothesis was checked by TD-DFT calculations for a simplified model of C57M. This model consists of isoalloxazin with a $–CH_2–S–CH_2–CH_3$ added in N(5) position, and the hydrogen removed from the C(4a) position. For the resulting radical, a TD-DFT/B3LYP spectrum out of its geometry-optimized D_0 ground state was calculated, and is shown in Fig. 7.

It is found that the lowest-energy absorption is at about 625 nm (1.98 eV), in reasonable agreement with the value of 675 nm (1.84 eV) observed in Ref. [54]. Also other features in the theoretical spectrum up to 300 nm, find their counterpart in experiment thus supporting the interpretation given in Ref. [54].

3.2. Adduct formation and spin–orbit coupling

3.2.1. A five-step model

The photochemical adduct formation in LOV domains was studied for a simplified model, with five independently optimized geometries A–E as shown in Fig. 8.

In the model, FMN is represented by the lumiflavin molecule (see Fig. 1), the adding cystein residue by mercaptomethan

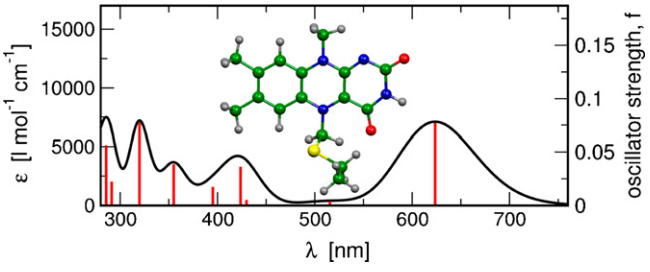

Fig. 7. Oscillator strengths f_i (right scale, sticks), extinction coefficient $\varepsilon(\lambda)$ (left scale, solid line) as a function of excitation wavelength λ (in nm) for the C57M-675 model (TD-UB3LYP)/6-31G(d)).

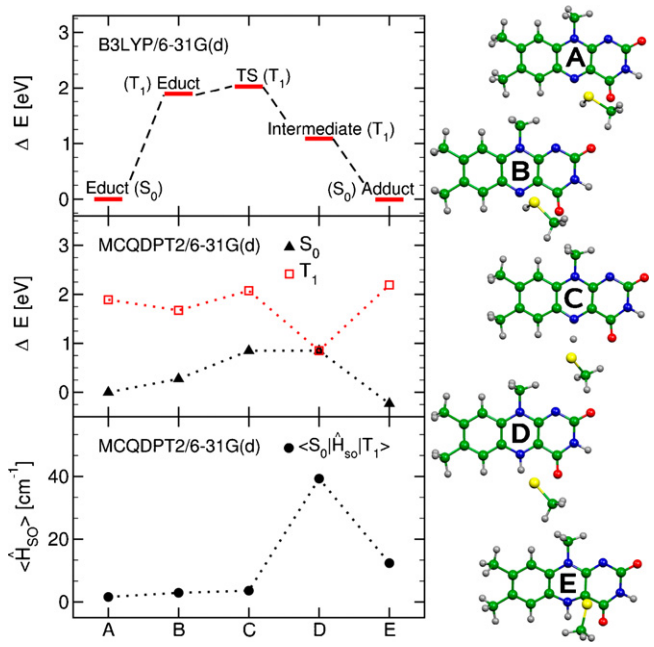

Fig. 8. Educt state (A and B), adduct state (E) and two intermediate steps (C and D) along the "reaction path" for adduct formation, see text. ΔE (in eV): energies relative to the S_0 energy of state A, for DFT(B3LYP) and MCQDPT2. $\langle S_0|\hat{H}_{so}|T_1\rangle$ (in cm^{-1}): spin–orbit coupling constants between S_0 and T_1, calculated with the MCQDPT2 method.

(MeSH). In a first step, all geometries (A–E) were optimized on the (U)B3LYP/6-31G(d) level of theory. The five structures represent different "snapshots" along the approximate reaction path for adduct formation. All of them are stationary points within the B3LYP method. The five structures are:

A. The educt configuration in its S_0 state, *i.e.* lumiflavin and a MeSH molecule pointing towards the flavin moiety ("educt S_0"). The distance between the sulfur atom of MeSH and the C(4a) atom of lumiflavin was restricted to 3.459 Å, in accordance with the crystal structure of *C. reinhardtii* [5].
B. The same restriction was applied in model B, which is analogous to model A except that the optimization was done for the triplet ground state, T_1("educt T_1"). For both structures A, B a S– H bond length of 1.35 Å was observed—the bond is intact.
C. A transition state between structures B and D, on the T_1 surface ("TS T_1"), was found with help of the QST3 method (see Section 2). No restrictions were applied on the geometry during the TS search. The transferring H atom is halfway between N(5) and S, with an elongated H– S distance of 1.53 Å. A single imaginary frequency along the hydrogen transfer coordinate was found, confirming the TS character. We also did IRC calculations in the T_1 state, following the reaction path from the TS in the direction of the H transfer coordinate. At the last point of the IRC which could be computed (before rapidly increasing spin contamination prevented convergence), the H– S distance was 2.17 Å and the N– H bond had formed. The resultant structure is very similar to structure D. The strong spin contamination along the late IRC, is indicative of the increasing multireference character of the wavefunction. All triplet states shown (B–D), however, have only minor spin contamination.
D. A state with H being already transferred to the N(5) position of lumiflavin, from its former position at the sulfur atom of MeSH. The optimization was done in the T_1 state. This is an intermediate state, henceforth also called "intermediate T_1".
E. The optimized adduct structure in its S_0 state, with the N– H and the S– C bonds formed ("adduct S_0").

In a second step, the geometries A–E were used for calculating the energy of the other spin state without reoptimization, *i.e.* T_1 if the structure was optimized in S_0 (for A and E), and S_0 if the optimization was done in T_1 (B, C and D). These 10 energies were then compared to those obtained (for the same geometries) with MCQDPT2/6-31G(d). The latter calculations serve to quantify the multireference character along the simplified "reaction path" (by comparison to the B3LYP results), and to compute the spin–orbit coupling between the $S_{0/1}$ and T_1 states. While the absolute energies obtained with MCQDPT2/6-31G(d) are not quantitative because the active space is probably too small, the multi-reference character of the reaction can still be addressed and also the spin–orbit coupling $\langle S_n|\hat{H}_{so}|T_1\rangle$ is expected to be at least qualitatively correct.

3.2.2. Adduct formation: energies

Table 3 contains all computed energies, relative to the educt (A) singlet ground state of the respective method, B3LYP/6-31G(d) or MCQDPT2/6-31G(d). Further shown in the table are the spin–orbit couplings between the S_0 and T_1 states, obtained with MCQDPT2/6-31G(d). Part of the information is also given in Fig. 8.

From the table we observe that the *energy differences*, relative to the S_0 state at point A and the according method, are reasonably close for both methods. Overall MCQDPT2 predicts smaller energy differences, for the S_0 and T_1 surfaces relative to B3LYP. S_0 is stabilized, up to 0.75 eV for point D. The T_1 energies observed by MCQDPT2 are approx. 0.25 eV lower than B3LYP, for points A, B and D along the path. The amount of stabilization seems directly connected to the multi reference character of the wave function. At point D, for example, the multireference character of the wavefunction is large, due to the biradical nature of the triplet intermediate (see below), and the nearby S_0 state. In this case MCQDPT2 pre-

Table 3
Five steps along the "reaction path" (A–E) for adduct formation, see text

	B3LYP/6-31G(d)		MCQDPT2/6-31G(d)		
	ΔE, S_0	ΔE, T_1	ΔE, S_0	ΔE, T_1	$\langle S_0\|\hat{H}_{so}\|T_1\rangle$ (cm^{-1})
A, educt, S_0	0.0	2.17	0.0	1.89	1.57
B, educt, T_1	0.26	1.89	0.27	1.67	2.91
C, TS, T_1	0.71	2.03	0.85	2.07	3.58
D, intermediate, T_1	1.60	1.09	0.85	0.84	39.29
E, adduct, S_0	0.0	2.98	−0.23	2.20	12.36

ΔE (in eV): energies relative to the educt S_0 state (A), calculated with DFT(B3LYP) or MCQDPT2. $\langle S_0|\hat{H}_{so}|T_1\rangle$ (in cm^{-1}): spin–orbit coupling constants between S_0 and T_1 states, calculated with MCQDPT2.

dicts clearly lower energy differences, relative to the S_0 state of A, than B3LYP, which does not, as a single-determinant method, properly account for the multireference behaviour. There is also a *qualitative* difference between MCQDPT2 and B3LYP at point D: While the former predicts the T_1 state to be more stable, the latter favours degenerated singlet and triplet ground states. Dittrich et al. found a similar behaviour to B3LYP with their (single-configuration) HF-based QM/MM calculation [29], *i.e.* a triplet ground state at points after the TS (C). Obviously, a multireference description changes this picture, which is also confirmed by earlier results of Domratcheva et al. [30].

A few points should be discussed in more detail. First, the reaction energies for adduct formation, *i.e.* the singlet energy differences $E(E) - E(A)$, are almost zero for B3LYP, and −22.2 kJ/mol (−0.23 eV) for MCQDPT2. This is in contrast to experimental findings for the LOV1 domain of Losi et al. [58], who found a clearly positive reaction enthalpy ΔH of +180 kJ/mol. For a more proper treatment we would have to determine enthalpy differences at ambient temperature, and account for details of the protein environment. One in fact finds even within our gas-phase model a positive reaction free enthalpy, $\Delta G(298.15\,\mathrm{K}) = +24.1$ kJ/mol (with B3LYP). An earlier DFT study for adduct formation in the gas phase also showed only a minor destablization for the adduct [28]. It has further already been shown that the inclusion of the protein environment, makes the reaction more endoenergetic [29]. The adduct forming cystein residue is connected to the protein backbone, the FMN moiety is attached to its binding pocket *via* hydrogen bonds and hydrophobic interactions. Adduct formation therefore causes changes in the protein structure, which most probably triggers the kinase activity of phot-proteins. The energetic of adduct formation is therefore also characterized by the protein environment. This could help to explain the difference between our approach for the gas phase reaction and the experimental data of Losi et al.

Second, the *transition state* (C) of the photocycle has some general characteristics. It is reached after a triplet has formed after photoexcitation of LOV-domains [8] by a first ISC. With the B3LYP functional, we find a transition state on the T_1 surface towards H transfer from the mercapto—(SH) group to N(5) of FMN. The calculated barrier height (energy difference between TS (C) and relaxed triplet educt (B)) is 13.5 kJ/mol (0.14 eV). With MCQDPT2, the activation barrier is found to be 38.6 kJ/mol (0.4 eV). The higher barrier for our MCQDPT2 calculation might be related to the fact that the B3LYP geometry was used, which is in fact no true transition state for the MCQDPT2 method, and because the surrounding protein is not exactly accounted for. A similar triplet reaction barrier of 43.3 kJ/mol was presented in a recent CASSCF/MCQDPT2 study concerning adduct formation in LOV domains [30]. However, recent spectroscopic investigations for the LOV-domains of *Arabidopsis thaliana* and of *Adiantum* phytochrome 3, showed smaller activation barriers of ($\leq$ 5 kJ/mol) for adduct formation [59,60]. Our results are therefore still above the experimental findings, but in better agreement than a Hartree-Fock based QM/MM approach by Dittrich et al. [29]. Their higher barrier of ca. 125 kJ/mol is probably due to the overestimation of barriers by Hartree-Fock.

As indicated in Fig. 8, no further barriers towards adduct formation were found, on the triplet surface. The intermediate triplet state (D) which we find, is more stable than the TS, but energetically still above the S_0 adduct state (E). Therefore, an unhindered reaction from the triplet intermediate (D) to the adduct in the ground state (E) can be assumed, in agreement with the recent findings in Ref. [30,29]. The just mentioned *intermediate*, D on the T_1 surface, is stabilized on the B3LYP and MCQDPT2 levels of theory relative to the triplet educt (B), by 77.2 kJ/mol (0.8 eV) and 79 kJ/mol (0.82 eV), respectively. Such a low-energy triplet intermediate was also found by Dittrich et al. in their QM/MM approach [29] and Domratcheva et al. [30]. Finally, the *adduct, E* is very high in energy, when calculated for the T_1 state, in agreement with earlier findings [28]. Therefore adduct formation has to take place in the S_0 state.

3.2.3. Spin–orbit coupling

3.2.3.1. Coupling between S_0 and T_1. From inspection of Fig. 8 and Table 3 it is clearly observed that the spin–orbit coupling between T_1 and S_0 states depends critically on the actual geometry. For geometries A and B, *i.e.* for arrangements early along the "reaction path", the coupling matrix elements are below 3.0 cm^{-1}. In both cases single determinants are a good description of the total wavefunction. For the singlet S_0, two electrons occupy the HOMO π-orbital, localized at lumiflavin, whereas in T_1 both the former HOMO π and LUMO π* orbitals are singly occupied, with parallel spin.

At the transition state geometry, C, the H atom is moving from S towards N(5). Therefore, the p-type orbital of sulfur is energetically destabilized and swaps position with the former, π-type HOMO of flavin: the latter becomes HOMO-1, while the new HOMO is a doubly occupied orbital localized at the methyl-S unit, in state S_0. The T_1 state, on the other hand, is a superposition of two dominating Slater determinants: the first one is similar to geometry B, *i.e.* the two flavin π and π* orbitals HOMO-1 and LUMO are each singly occupied. In the second, HOMO and LUMO orbitals are singly occupied. Therefore, the previously purely flavin-type triplet T_1 gains some biradical character, and some charge transfer occurs from the MeS unit, to flavin. The spin–orbit coupling strength between S_0 and T_1 appears to be slightly increased, to 3.6 cm^{-1}.

The spin–orbit coupling increases strongly to almost 40 cm^{-1} for point D. Here, for the intermediate, the H atom is already covalently bound at the N(5) position of FMN, with a N(5)–H distance of 1.03 Å. The HOMO and now also the HOMO-1 orbital show main contributions for the S-atom of the MeS unit. The highest π orbital of flavin is shifted to the HOMO-2 position. The LUMO is still dominantly a π* orbital of lumiflavin, and has only small coefficients at the MeS unit. The frontier orbitals are shown in Fig. 9. The T_1 state is now entirely characterizable as a biradical, with HOMO-1 and LUMO singly occupied. The S_0 state, on the other hand, is composed of three, almost equally weighted configuration state functions. These are, (i) a "ionic" determinant with a doubly occupied HOMO, located at MeS, *i.e.* formally MeS^- and $flavin^+$. (ii) A second, also

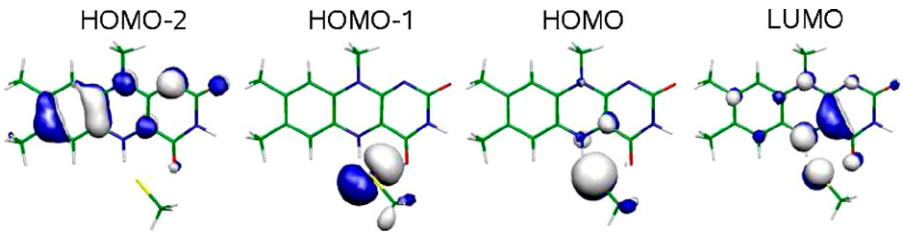

Fig. 9. RHF/6-31G(d) orbital shape for HOMO-2, HOMO-1, HOMO and LUMO at geometry D (see Fig. 8).

ionic configuration consists of singly occupied HOMO-2 and LUMO orbitals, *i.e.* MeS^+ and $flavin^-$. (iii) The third configuration consists of singly occupied HOMO-1 and LUMO orbitals, and contributes some biradical character also for the S_0 state. The same biradicalic HOMO-1/LUMO description was seen for T_1. Therefore, by sharing the same orbitals and the biradical character, mixing of triplet and singlet states becomes very efficient. The spin density, being partially localized at the heavy sulfur atom, causes the high spin–orbit coupling strength at point D. For state D, MCQDPT2 shows the smallest T_1–S_0 energy gap, of about 1.0 kJ/mol (0.01 eV). According to perturbation theory, a small energy gap increases the probability of an ISC event.

Finally, for the *adduct state* (E) geometry, the spin–orbit coupling decreases again to about 12 cm^{-1}. The S_0 state is dominated by a configuration with a doubly occupied flavin π orbital. The T_1 state is characterized by a $HOMO^1$ $LUMO^1$ configuration. The LUMO consists of π-shaped contributions from lumiflavin and additional p-type orbitals of S. The LUMO is antibonding with respect to the S–C(4a) bond, which explains the observed energetic destabilization of the triplet adduct.

3.2.3.2. Coupling between S_1 and T_1. We also calculated the potential surface for the first excited singlet state (S_1) and spin–orbit coupling strength between S_1 and T_1 states. We won't discuss the results in detail but mention the most important findings. The energy differences between S_0 and S_1 are within 0.2 eV accuracy compared to the spectroscopic data [4], for educt (A) and adduct state (E). The shape of S_1 energies follow qualitatively those for T_1 and stays $\sim$ 0.5 eV above it at points A, B and E. For the transition state (C) and the intermediate state (D) small energy gaps between S_0 and T_1 of 0.05 eV and 0.2 eV were calculated, respectively.

The spin–orbit coupling strength between S_1 and T_1 is maximal at the intermediate point (D) with about 180 cm^{-1} and below 5 cm^{-1} otherwise. At point D, the S_1 state is partly characterized by a HOMO-1, LUMO configuration, which is also the dominant one for the T_1 state at position D. This is taken as reason for the high coupling rate between S_1 and T_1 state. HOMO-1, LUMO orbitals are shown in Fig. 9.

3.2.3.3. Summary. To summarize, we presented a five-step "reaction path" modeling the FMN-C(4a)-cysteinyl adduct formation during the photocycle of LOV domains [4]. After initial photoexcitation and a first ISC to T_1, a neutral H atom is transferred from the sulfur atom to the N(5) position of flavin. This costs only little activation energy. The biradical character of the reaction on the triplet surface is clearly emergent, from the transition state (C) up to an intermediate state (D) at which the H transfer is complete. The H transfer increases the spin density at the sulfur atom, leading to a second ISC. We find that the second ISC occurs right after the H transfer took place. This is the prerequisite for C(4a)–S bond formation in the S_0 state, which cannot occur on the triplet surface because of its strong repulsive character. The mechanism is not only consistent with previous work [28–30], it also helps to explain the observed blocking of adduct formation, when cystein is replaced by serin [4]: ISC is less efficient, when S is replaced by O. Another reason is energetics: the S– H bond is easier to break than the O– H bond [28].

4. Conclusions

In the first part of this paper, the effects of a solvent or a protein environment on the absorption spectra of lumiflavin, were studied with the help of time-dependent density functional theory. The polarizability of an environment, the formation of H-bond between chromophore and environment, and the geometric confinement of the chromophore in a protein binding pocket all lead to red-shifts of the lowest visible transitions $S_0 \rightarrow S_1$, S_2, and S_3. As a specific example, we find that the S_2 band position depends stronger on H bonding than S_1, in agreement with experiment [17,22]. The vibrational fine structure of the S_1 band is caused by vibrations of the central ring of lumiflavin, after $\pi \rightarrow \pi^*$excitation. At last, a fairly good agreement between theoretical and experimental spectra was achieved with a simple model in which, however, H-bonding aminoacids were explicitly included, the polarizability of the environment and distortions by the protein binding pocket were accounted for. Also, variations of the spectral properties in a mutant (C57M-675), could be accounted for by quantum mechanical calculations.

In the second part of our work, spin–orbit coupling constants were obtained on the basis of multireference perturbation theory and a Breit–Pauli coupling Hamiltonian. A simplified "reaction path" for the addition reaction in LOV1 domains was constructed and 5 geometries considered. The second ISC event, from the triplet to the singlet ground state, during the LOV-photocycle is connected to the biradical character of these states, in particular after the transition state towards H transfer on the triplet surface has been passed.

Despite the present work sheds light on some details of the electronic properties and photoreaction mechanisms of biological photoreceptors, this is only a small step towards a more complete theory. From the latter, we expect also a quantitative treatment of the timescales of radiative and non-radiative

transitions, and, eventually, the nuclear dynamics on multi-dimensional, coupled potential energy surfaces. Exciting flavins, therefore, will be an exciting topic also for the future.

Acknowledgments

We acknowledge fruitful discussions with B. Dick (Regensburg), P. Hegemann (Berlin) and L. Lustres (Berlin). Support by the collaborative research program GoFORSYS, and by the Fonds der Chemischen Industrie, is gratefully acknowledged.

References

[1] P. Hegemann, M. Fuhrmann, K. Suneel, J. Phycol. 37 (2001) 668–676.
[2] J. Christie, T. Swartz, R. Bogomolni, W. Briggs, Plant J. 32 (2002) 205–219.
[3] W. Briggs, et al., Plant Cell 13 (2001) 993–997.
[4] T. Kottke, J. Heberle, D. Hehn, B. Dick, P. Hegemann, Biophys. J. 84 (2003) 1192–1201.
[5] R. Fedorov, I. Schlichting, E. Hartmann, T. Domratcheva, M. Fuhrmann, P. Hegemann, Biophys. J. 84 (2003) 2474–2482.
[6] C. Kay, E. Schleicher, A. Kuppig, H. Hofner, R. Wolfhart, et al., J. Biol. Chem. 278 (2003) 10973–10982.
[7] D. Nozaki, T. Iwata, T. Ishikawa, T. Todo, S. Tokutomi, H. Kandori, Biochemistry 43 (2004) 8373–8379.
[8] W. Holzer, A. Penzkofer, M. Fuhrmann, P. Hegemann, Photochem. Photobiol. 75 (2002) 479–487.
[9] M. Sun, T. Moore, P. Song, J. Am. Chem. Soc. 94 (1972) 1730–1740.
[10] P. Song, T. Moore, J. Am. Chem. Soc. 90 (1968) 6507–6514.
[11] J. Wouters, F. Durant, B. Champagne, J.-M. André, Int. J. Quant. Chem. 64 (1997) 721–733.
[12] E. Gross, J. Dobson, M. Petersilka, Topics in Current Chemistry (181): Density Functional Theory II: Relativistic and Time Dependent Extensions, vol. 181, Springer, Berlin, 1996.
[13] A. Becke, Phys. Rev. A 38 (1988) 3098–3100.
[14] C. Neiss, P. Saalfrank, M. Parac, S. Grimme, J. Phys. Chem. A 107 (2003) 140–147.
[15] E. Sikorska, I. Khmelinskii, J. Koput, J. Bourdelande, M. Sikorski, J. Mol. Struct. 697 (2004) 137–141.
[16] M. Kowalczyk, M. Sikorska, I. Khmelinskii, J. Komasa, M. Insinska-Rak, M. Sikorski, J. Mol. Struct. 756 (2005) 47–54.
[17] E. Sikorska, I. Khmelinskii, W. Prukala, S. Williams, M. Patel, D. Worral, J. Bourdelande, J. Koput, M. Sikorski, J. Phys. Chem. A 108 (2004) 1501–1508.
[18] K. Dudley, A. Ehrenberg, P. Hemmerich, F. Müller, Helv. Chim. Acta 47 (1964) 1354–1383.
[19] G. Hutchison, M. Ratner, T. Marks, J. Phys. Chem. A 106 (2002) 10596–10605.
[20] C. López, O. Faza, S. Estévez, A. de Lera, J. Comput. Chem. 27 (2005) 116–123.
[21] S. Grimme, M. Waletzke, J. Chem. Phys. 111 (1999) 5645–5655.
[22] P. Heelis, Chem. Soc. Rev. 11 (1982) 15–39.
[23] H. Guo, T. Kottke, P. Hegemann, B. Dick, Biophys. J. 89 (2005) 402–412.
[24] S. Vaish, G. Tollin, J. Bioenerg. Biomembr. 1 (1970) 181–192.
[25] E. Schleicher, R. Kowalczyk, C. Kay, P. Hegemann, A. Bacher, M. Fischer, R. Bittl, G. Richter, S. Weber, J. Am. Chem. Soc. 126 (2004) 11067–11076.
[26] G. Richter, S. Weber, W. Römisch, A. Bacher, M. Fischer, W. Eisenreich, J. Am. Chem. Soc. 127 (2005) 17245–17252.
[27] R. Bittl, C. Kay, S. Weber, P. Hegemann, Biochemistry 42 (2003) 8506–8512.
[28] C. Neiss, P. Saalfrank, Photochem. Photobiol. 77 (2003) 101–109.
[29] M. Dittrich, P. Freddolino, K. Schulten, J. Phys. Chem. B 109 (2005) 13006–13013.
[30] T. Domratcheva, R. Fedorov, I. Schlichting, J. Chem. Theory Comput. 2 (2006) 1565–1574.
[31] R. Ditchfield, W. Hehre, J. Pople, J. Chem. Phys. 54 (1971) 724–728.
[32] C. Martin, M. Tsao, C. Hadad, M. Platz, J. Am. Chem. Soc. 124 (2002) 7226–7234.
[33] J. Rodríguez-Otero, E. Martínez-Núñez, A. Peña Gallego, S. Vázquez, J. Org. Chem. 67 (2002) 6347–6352.
[34] E. Cancès, B. Mennucci, J. Tomasi, J. Chem. Phys. 107 (1997) 3032–3041.
[35] V. Barone, M. Cossi, J. Tomasi, J. Chem. Phys. 107 (1997) 3210–3221.
[36] J. Pascual-Ahuir, E. Silla, J. Comput. Chem. 11 (1990) 1047–1060.
[37] G. Ullmann, E. Knapp, Eur. Biophys. J. 28 (1999) 533–551.
[38] M.J. Frisch, G.W. Trucks, H.B. Schlegel, G.E. Scuseria, M.A. Robb, J.R. Cheeseman, J.A. Montgomery, Jr., T. Vreven, K.N. Kudin, J.C. Burant, J.M. Millam, S.S. Iyengar, J. Tomasi, V. Barone, B. Mennucci, M. Cossi, G. Scalmani, N. Rega, G.A. Petersson, H. Nakatsuji, M. Hada, M. Ehara, K. Toyota, R. Fukuda, J. Hasegawa, M. Ishida, T. Nakajima, Y. Honda, O. Kitao, H. Nakai, M. Klene, X. Li, J.E. Knox, H.P. Hratchian, J.B. Cross, V. Bakken, C. Adamo, J. Jaramillo, R. Gomperts, R.E. Stratmann, O. Yazyev, A.J. Austin, R. Cammi, C. Pomelli, J.W. Ochterski, P.Y. Ayala, K. Morokuma, G.A. Voth, P. Salvador, J.J. Dannenberg, V.G. Zakrzewski, S. Dapprich, A.D. Daniels, M.C. Strain, O. Farkas, D.K. Malick, A.D. Rabuck, K. Raghavachari, J.B. Foresman, J.V. Ortiz, Q. Cui, A.G. Baboul, S. Clifford, J. Cioslowski, B.B. Stefanov, G. Liu, A. Liashenko, P. Piskorz, I. Komaromi, R.L. Martin, D.J. Fox, T. Keith, M.A. Al-Laham, C.Y. Peng, A. Nanayakkara, M. Challacombe, P.M.W. Gill, B. Johnson, W. Chen, M.W. Wong, C. Gonzalez, J.A. Pople, Gaussian Inc., Wallingford, CT, 2004.
[39] H. Nakano, J. Chem. Phys. 99 (1993) 7983–7992.
[40] H. Nakano, Chem. Phys. Lett. 207 (1993) 372–378.
[41] M. Schmidt, K. Baldridge, J. Boatz, S. Elbert, M. Gordon, J. Jensen, S. Koseki, N. Matsunaga, K. Nguyen, S. Su, T. Windus, M. Dupuis, J. Montgomery, J. Comput. Chem. 14 (1993) 1347–1363.
[42] D.G. Fedorov, J.P. Finley, Phys. Rev. A 64 (2001) 042502–042502-10.
[43] C. Teichteil, M. Pelissier, F. Spiegelmann, Chem. Phys. 81 (1983) 273–282.
[44] B. Brandow, Rev. Mod. Phys. 39 (1967) 771–825.
[45] D.G. Fedorov, M.P. Gordon, J. Chem. Phys. 112 (2000) 5611–5623.
[46] C. Peng, P. Ayala, H. Schlegel, M. Frisch, J. Comput. Chem. 17 (1996) 49.
[47] C. Gonzalez, B. Schlegel, J. Phys. Chem. 94 (1990) 5523–5527.
[48] A. Dreuw, J. Weisman, M. Head-Gordon, J. Chem. Phys. 119 (2003) 2943.
[49] E.C. Lim, J. Phys. Chem. 90 (1986) 6770–6777.
[50] E. Sikorska, I. Khmelinskii, D. Worrall, J. Koput, M. Sikorski, J. Fluoresc. 14 (2004) 57–64.
[51] E. Sikorska, I. Khmelinskii, J. Koput, J. Bourdelande, M. Sikorski, J. Mol. Struct. 697 (2004) 137–141.
[52] G. Kleywegt, A. Brünger, Structure 4 (1996) 897–904.
[53] M.A. Petrukhina, K. Andreini, J. Mack, T.S. Lawrence, J. Org. Chem. 70 (2005) 5713–5716.
[54] T. Kottke, B. Dick, R. Fedorov, I. Schlichting, R. Deutzmann, P. Hegemann, Biochemistry 42 (2003) 9854–9862.
[55] A. Scott, L. Radom, J. Phys. Chem. 100 (1996) 16502–16513.
[56] S. Zilberg, Y. Haas, S. Shaik, J. Phys. Chem. 99 (1995) 16558–16565.
[57] K. Wiberg, J. Phys. Chem. 97 (1993) 13586–13597.
[58] A. Losi, T. Kottke, P. Hegemann, Biophys. J. 86 (2004) 1051–1060.
[59] D. Nozaki, T. Iwata, H. Tokutomi, S. an Kandori, Chem. Phys. Lett. 410 (2005) 59–63.
[60] K. Zikihara, T. Iwata, D. Matsuoka, H. Kandori, T. Todo, S. Tokutomi, Biochemistry 45 (2006) 10282–10837.